RSC Advances

ROYAL SOCIETY OF CHEMISTRY

www.rsc.org/advances

Journal Name

RSCPublishing

ARTICLE

F-assisted Synthesis of Hierarchical ZSM-5 Zeolite for Methanol to Propylene Reaction: *b*-Oriented Thinner Dimensional Morphology

Lanlan Zhang,[a] Yu Song,[a] Guodong Li,[a] Qing Zhang,[a] Shaolong Zhang,[a] Jun Xu,[b] Feng Deng,[b] and Yanjun Gong*[a]

Cite this: DOI: 10.1039/x0xx00000x

Received 00th January 2012,
Accepted 00th January 2012

DOI: 10.1039/x0xx00000x

www.rsc.org/

Under neutral fluoride medium at 373 K, a facile strategy has been developed to synthesis hierarchical ZSM-5 zeolite (M-ZSM-5) by using solid silica source in dense system. The resulting material shows hexagonal lamellar shape with *b*-oriented thinner dimension and bi-modal porosity containing MFI micropore and intracrystal mesopore. The effect of synthesis factors, such as NH_4F/SiO_2, H_2O/SiO_2, crystallization temperature and time, on the zeolite morphology and size are studied and its primary crystallization process is proposed. Through varying synthesis parameters, the crystal size could be tuned with the aspect ratio at a range of 6.2-12. Typically, M-ZSM-5 with thinner thickness (100 nm) and a high aspect ratio (AR=12) has highly effective catalytic performance in methanol to propylene (MTP) reaction. Compared to bulk C-ZSM-5 sample obtained from hydroxyl system, M-ZSM-5 shows higher selectivity to propylene (45.1% vs. 38.1%) and butylene (27.2% vs. 21.3%), especially prolonged catalytic lifetime (224 h vs. 98 h). This enhanced performance could be contributed to the optimized acidity and superior diffusivity of M-ZSM-5 with lamellar morphology and bimodal porosity, which are crucial for suppressing secondary reactions and inhibiting coke deposition.

1. Introduction

Methanol to propylene (MTP) process, originally developed by Lurgi's company, provides an alternative route for the production of propylene, which attracts more scientific and applicable interests.[1-3] Zeolite ZSM-5 with intricate channel, adjustable acidities and high thermal/hydrothermal stability has been proved to be a remarkably effective material in MTP reaction.[4, 5] Recently, the theoretical and experimental results give many new insights into the extremely complex reaction network[6-8] and the underlying interplay between catalyst microstructure and its MTO/MTP performance.[9-11]

The most accepted "dual-cycle" mechanism for MTO/MTP reaction suggests that ethylene is formed from the lower methylbenzenes in the aromatics-based cycle whereas propylene is generated through olefin-based cycle by alkene methylations, and the light olefins can be further converted to alkanes and aromatics by alkylation, cracking, hydrogen transfer and cyclization reactions.[12, 13] The narrow channels strongly impose restriction on the transport of product molecules, leading the increase of secondary reactions. Therefore, this implies that the improvement of diffusivity would be benefit to increase the propylene selectivity and reduce the coke deposit.[14, 15]

Some strategies have been adopted to reduce the diffusion resistance of the pure microporosity in ZSM-5 zeolite. Decreasing the crystal size to nanometer scale and introducing an auxiliary mesopores into zeolite crystals are benefit to shorten the diffusion path length and improve the accessibility to the internal surface.[16, 17] However, the separation from mother liquor is a big difficulty for the nano-sized zeolite in large scale, and the preparation of hierarchical zeolite requires multiple synthesis steps and/or costs expensive organic templates. ZSM-5 zeolite possesses an anisotropic framework with two intersecting 10-membered ring channels, among which straight channels parallel to *b*-axis and zig-zag channels parallel to *a*-axis.[18] Guest molecular can transfer through the two channels in the zeolite crystal for the process of catalytic reaction or separation. And faster diffusion rate can be observed in the direction of *b*-axis due to the diffusion anisotropy.[19-21] Ryoo's group synthesized ZSM-5 nanosheets consisting of 2 nm-thick layers along the *b*-axis dimension,[22, 23] which performed high activity in large molecular reaction because the specific crystal with *b*-axis thin layers facilitated the accessibility of acid sites at the exteriors or pore mouths. According to our previous work,[24] the high propylene

selectivity and the low deactivation rate over ZSM-5 nanosheets could mainly be ascribed to its unique morphology with the shorten diffusion path length in MTP reaction. Further insightful studies also embodied the concept of 2D zeolite morphology and its importance in catalysis.[25] The ultra-thin nanosheets would lead to lower hydrothermal/physical stability, but it arouse an inspiration for controlling the crystal growth rates along the three crystallographic axes, forming ZSM-5 zeolite with the thinner *b*-dimension.

Many works evidenced that synthesis conditions (such as molar composition, Si or Al raw materials, templates, additive, pH value, crystallization method and time) have marginal effects on the kinetics and thermodynamics of crystal growth, which accounts for the morphology, preferential growth and orientation of the MFI zeolite crystals.[26, 27] By using dimers and trimers of TPAOH as structure-directing agent (SDA), Bonilla et. al found the growth rates of ZSM-5 crystals along each axes of a*b*c direction depend on each amount of SDAs used in the hydroxyl system.[28] Combining the utilization of co-solvent of diols and the microwave heating, Chen et al. fabricated silicate-1 crystals with tuneable sizes, shapes, and the aspect ratios.[29] Xiao's group synthesized the TS-1 crystals and found that the growth rate of MFI crystals along the *b*-axis can be suppressed by the addition of urea.[30, 31]

Recently, a significant progress in zeolite synthesis has been made when fluoride ions replace hydroxyl anions as a mineralizer, largely extending the synthetic pathway of zeolite.[32] It is believed that F atoms occluded inside small cages in MFI structure progressively which modified the neighboring silicon[33] to affect zeolite morphology, pore structure and acid properties, resulting in an enhancement of catalytic activity and selectivity. Arichi et al. prepared ZSM-5 zeolite with star-like /hedgehog-like morphology by using polymeric and monomeric silica source with certain ratio of F/Si.[34] And also, under fluoride medium, crystal size of ZSM-5 can easily be controlled[35] and the crystals with *b*-axis oriented are synthesized by the addition of co-template.[36] For instance, Dose et al. synthesized Silicate-1 zeolites with tuned crystal size ranging from 0.4 to 30 μm along the *b* direction.[37] Yao et al. prepared Silicalite-1 with plate-like morphology with varying axes thickness and they found that anisotropic growth of crystal faces was mainly governed by the concentration of NH_4F in the gels.[38] ZSM-5 zeolites obtained in fluoride and hydroxide medium were comparatively evaluated in MTO/MTP reactions.[39, 40] The large ZSM-5 crystals with size of 15-20 μm obtained in fluoride medium exhibited lower B acid sites density, thus giving rise to a high propylene to ethylene (P/E) ratio in MTO reaction.[40] Through seed addition in F medium at 443 K, the resulting ZSM-5 exhibits cubic small particles, fewer structure defects and thus optimized acidity, which is favourable for high initial activity and resistance to deactivation in MTH reaction.[41]

Herein, under neutral fluoride medium at 373 K, hierarchical ZSM-5 zeolite was obtained by using single TPABr template, solid silica source and thus formed dense system. The resulting material showed hexagonal lamellar shape with thinner *b*-axis dimension, containing the bi-modal porosity, which performed excellent catalytic performance in the MTP reaction. Influencing factors in the crystallization process are systematically discussed for finely tuning the zeolite crystal size, aspect ratio and microstructure. In addition, the primary synthesis mechanism of the ZSM-5 crystal was proposed.

2. Experimental

2.1 Synthesis of hierarchical ZSM-5 zeolite in fluoride medium

Hierarchical ZSM-5 zeolite and the counterpart ZSM-5 sample were synthesized by using the following chemicals as raw materials. Solid silica gel (SiO_2, 99 wt. %) was purchased from Qingdao Haiyang Chemical Co. (P.R. China). Sodium aluminate ($NaAlO_2$, 41 wt.% Al_2O_3), aluminum sulfate ($Al_2(SO_4)_3{\cdot}18H_2O$, >98 wt.%), tetrapropylammonium bromide (TPABr, >98 wt.%) were purchased from Sinopharm Chemical Reagent Co., Ltd. (P.R. China). Ammonium fluoride (NH_4F, >99 wt. %) and NaOH were obtained from Beijing Yili Co. (P.R. China).

A typical synthesis for the hierarchical ZSM-5 zeolite in fluoride medium is performed as following procedure. NH_4F was completely dissolved in deionized water and $Al_2(SO_4)_3{\cdot}18$ H_2O, and TPABr were added into the fluoride solution. After that, SiO_2 was added into the mixture slowly under stirring with the final mole ratios: SiO_2 : 0.02 Al_2O_3 : 0.048 TPABr : 0.8 NH_4F : 6 H_2O. The pH was adjusted to 6.5-7.5 by the dropwise addition of hydrochloric acid solution (HCl, 1 M) under vigorous stirring, while the accurate pH paper was used for the pH adjustments. After aging at 323 K for 12 h, the mixture was transferred into a Teflon-lined stainless-steel autoclave and crystallized at 373 K and 453 K for a specific period, respectively. After crystallization, the obtained product was filtered, thoroughly washed with deionized water, dried overnight at 393 K. By varying preparation parameters, such as NH_4F/SiO_2 ratio, H_2O/SiO_2 ratio, crystallization temperature and time, different samples were obtained as the same procedure, which parameters are listed as in Table 1 and named A-F alphabetically.

For comparison, the conventional ZSM-5 zeolite was prepared in alkaline system. $NaAlO_2$, SiO_2, TPABr and NaOH were orderly added into deionized water with the mole ratio as follows: SiO_2 : 0.0033 Al_2O_3 : 0.24 TPABr : 0.4 Na_2O : 28 H_2O. Finally, the mixture was crystallized at 453 K for 48 h and the product was collected by filtration, washed thoroughly and dried overnight at 393 K.

To obtain protonic form zeolites, the synthesized products were calcined at 823 K for 6 h to remove the organic template, and then ion-exchanged twice in NH_4Cl solution (1 M) at 363 K for 2 h, followed by calcination at 823 K for 6 h. After calcined and ion-exchange, fluoride anions compensating TPA^+ in the as-synthesized ZSM-5 are released.

2.2 Catalyst characterization

X-ray diffraction (XRD) patterns were determined by a Bruker D8 Advance X-ray diffractometer using Cu Kα radiation operated at 40 kV and 30mA with the range of 2 θ = 5°~50° and at a scanning rate of 2°/min. The relative crystallinity of the samples was calculated by comparing the sum of the characteristic peaks area between 2θ = 22.5°-25° with that of the commercial ZSM-5 zeolite (Nankai Catalyst Plant, China, the crystallinity was considered to be 100%). The element compositions of the samples were measured using AxiosmAX X-ray fluorescence analyser (XRF).

Scanning electron microscopy (SEM) images were performed on Quanta 200F for the morphology and crystal size of the samples. Transmission electron microscopy (TEM) images were carried out in a Tecnai G^2 F20 instrument with operating at 200 kV.

Nitrogen adsorption-desorption isotherms were measured on Micromeritics ASAP 2020 instrument at 77 K. Prior to measurements, the samples were degassed at 573 K under vacuum for 4 h. Specific surface area is calculated by the BET equation. The total pore volume is based on the nitrogen adsorbed volume at P/P_0=0.99. The external surface area is calculated via the t-plot method. The mesopores size distribution is analyzed by Barrett-Joyner-Halenda (BJH) method to the desorption branch of the isotherms.

Temperature programmed desorption of ammonia (NH_3-TPD) measurements were performed on a fixed-bed reactor with a thermal conductivity detector (TCD) for measuring the acidity. The samples (0.1 g, particle size 20-40 mesh) were first pre-treated at 873 K for 1 h in a flow of He, then cooled down to 373K, and saturated in NH_3 for 30 min. Finally, the samples were conducted in He-flow by raising the temperature from 373 K to 873 K at a rate of 10K min^{-1}.

Solid state ^{19}F magic angle spinning nuclear magnetic resonance spectroscopy (MAS-NMR) was conducted on Bruker 500 MHz spectrometer at a resonance frequency of 470.95 MHz using 2.5 mm rotor. In the experiment, ^{19}F MAS NMR spectrum was recorded with a pulse width of 1 μs and spinning rate of 23 kHz. $CFCl_3$ was used as reference for the chemical shift of ^{19}F.

2.3 Catalyst evaluation

The MTP reaction was conducted in a fixed-bed micro-reactor with an inner diameter of 8 mm at 743 K under atmospheric pressure. For each test, catalyst (H form zeolite samples,1 g, particle size 20-40 mesh) was loaded to the reactor. The mixture of methanol and water with the molar ratio of 1:1 was fed into a reactor and the weight hourly space velocity (WHSV) was set at 3 h^{-1}. The products were analyzed by an online gas chromatograph (Agilent GC 7890) equipped with a flame ionization detector (FID) and an HP-PLOT Q capillary column. Methanol and DME were considered as reactants in the calculation of conversion and selectivity.

After methanol conversion, the amount of generated coke in the ZSM-5 catalysts was determined by thermogravimetric (TGA) analysis, which was performed on a TG-DTAXSTAR6000 instrument. In a typical experiment, the TGA curve was recorded as the catalyst (10 mg) was heated from 298 K to 1073 K with a heating rate of 10 K/min.

3. Results and Discussion

3.1 Synthesis of ZSM-5 zeolites in the fluoride medium

In the mixture gels, the solubility of solid SiO_2 and thus formed silica /aluminum species depend on the acidic/basic property in medium. To a certain extent, the crystallization process is governed by pH value, which further affects the zeolite morphology and porosity.[42] Due to fluoride as an effective mineralizer and a structure-directing agent, ZSM-5 synthesis could accomplish under neutral/weakly acidic condition by using fluoride route, differing from traditional synthesis conducted in alkaline solution.[43] Herein, experiments were performed in the presence of NH_4F to synthesize ZSM-5 zeolite at optimal pH=6.5-7.5, NH_4F/SiO_2, H_2O/SiO_2 and crystallization temperature and time. The relative crystallinity, crystal size of the prepared ZSM-5 samples and corresponding synthesis parameters are summarized in Table 1.

Table 1. Synthesis of ZSM-5 samples in the fluoride medium

No.	NH_4F /SiO_2	H_2O /SiO_2	Temp. [K]	Time [h]	RC [a] [%]	Crystal size [b] [L×W×T] μm	AR [c]
A	0.6	6	373	72	62	/ × / × 0.10	-
B	0.8	6	373	72	98	1.6 × 0.8 × 0.10	12.0
C	1.2	6	373	72	90	2.8 × 1.5 × 0.25	8.6
D	1.6	6	373	72	85	3.6 × 2.0 × 0.45	6.2
E	0.8	20	373	72	78	3.8 × 1.8 × 0.35	8.0
F	0.8	6	453	12	90	2.4 × 1.0 × 0.20	8.5

[a] Denoted to Relatively Crystallinity. [b] The average crystal size of ZSM-5 crystals with length (L), width (W) and thickness (T) are estimated by high resolution SEM images. [c] Denoted to the aspect ratio,[37] AR = (L+W)/2T.

By varying NH_4F/SiO_2 ratios from 0.6, 0.8, 1.2 to 1.6, XRD patterns (Figure 1(i)) show that all samples consist of MFI phase, and the crystallinity of the samples with varying NH_4F/SiO_2 is 62%, 98%, 90% and 85%, respectively. This indicates that a small amount of fluoride is disadvantageous to the formation of ZSM-5 zeolite. In the meanwhile, the excessive fluoride also interrupts the electronic interaction between the anion silicates and cation TPA^+ in the synthesis gel, leading to the production of some miscellaneous crystals.[44] Hence, the appropriate amount of fluoride is conducive to promoting the formation of Si-O-Si bond, influencing the hydrolysis and condensation of silicates during the crystal growth process, which would play an important role in the ZSM-5 morphology as well.

Figure 1(ii) presents the morphologies of the synthesized ZSM-5 samples with varying NH_4F/SiO_2 ratios. Figure 1(iii) shows a schematic identifying the crystal size and corresponding crystal faces. As the NH_4F/SiO_2 ratio is 0.6, the crystals display overall inter-grown and connected lamellar shape with the thickness less than 100 nm. With the increasing ratio of NH_4F/SiO_2 to 0.8, the crystals gradually grow to individual and regularly hexagonal lamellar morphology featuring a high aspect ratio (AR = 12.0). The average size of the length and width are about

1.6 and 0.8 μm and the thickness along *b* axis is only 0.1 μm. Some inter-grown hexagonal plates appear when NH_4F/SiO_2 ratio increases to 1.2, and the crystal size is increased to 2.8 × 1.5 × 0.25 μm with AR of 8.6. Further increase of F^- concentration, the highly dispersed particles with inter-grown ellipse shape are gotten. The crystal size becomes larger (3.6 × 2.0 × 0.45 μm), while AR is lower of 6.2.

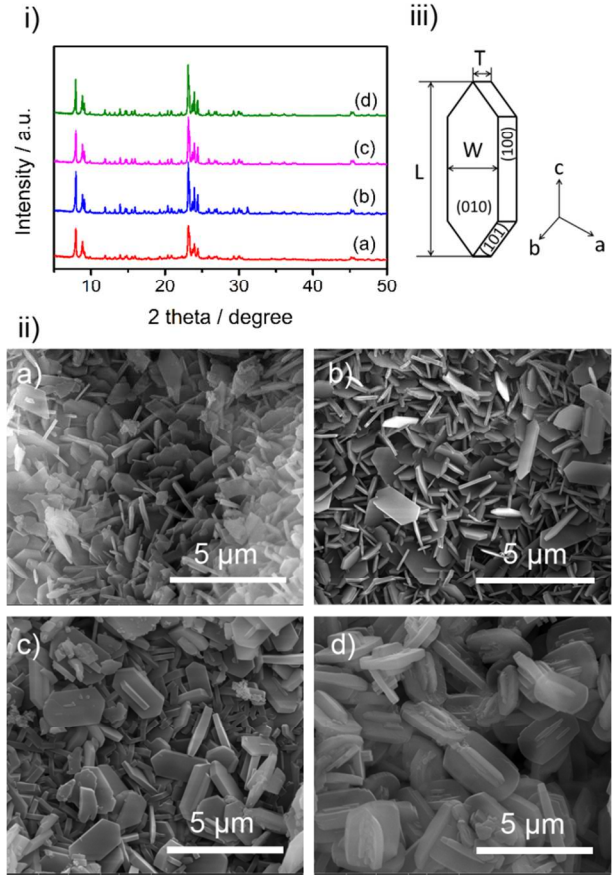

Figure 1. i) XRD patterns and ii) SEM images of ZSM-5 samples with NH_4F/SiO_2 ratios of a) 0.6, b) 0.8, c) 1.2 and d) 1.6, respectively. iii) Crystal dimensions and the corresponding crystal faces.

ZSM-5 crystal sizes of length, width and thickness are increase but the aspect ratio decreases with increasing F^- concentration, which indicates that the addition of fluoride anions affects the crystal growth rate along each crystal face. According to the Bravais–Friedel–Donnay–Harker (BFDH) law,[45, 46] the growth rates along a crystallographic direction is inversely proportional to its interplanar distance d_{hkl}, the fastest growth direction of MFI zeolite is always along the *c*-axis of the crystals. For the synthesis of MFI zeolite with TPA^+ as structure-directing agent, the typical morphology of ZSM-5 crystals is coffin shaped with the order of crystal dimensions $L_c > L_a > L_b$, where L_i indicates crystal size along *i* axis.[28] In the initial stage, zeolite nucleation is occur on the surface of gel spheres and the crystals are more likely to oriented with their *ac*-plane parallel to the gel sphere surface.[47, 48] It is believed that the dissolution and depolymerization of Si sources are closely associated with the concentration of fluoride anions, and the supersaturation degree of silicate species in the synthesis gels influences the growth rate of the crystal along the *b*-axis.[49] When employing solid silica as silica source under the low F^- concentration, the dissolution rate of Si is relatively slow and the formation of hydroxylated silica species could be controlled, thus the adsorption of silica species on the nuclei interface is inhibited. Therefore, the crystal growth rate in the direction along *b* axis is slow and results in the formation of ZSM-5 crystals with thinner dimensional morphology. With the increasing fluoride concentration in the gels, the dissolution rate of silicon is increased and more silica nutrient can be supplied from solution. The crystal growth rate is accelerated in all directions to form inter-grown ellipse crystals with the enhancement surface energy from the electrostatic forces between F^-, TPA^+ and Si species. Herein, it is implied that F^- concentration has intense effect on the dissolution of Si source and indirectly control the growth rate of crystal face to form ZSM-5 crystals with *b*-oriented morphology.

Water content affects the dissociation and migration of raw materials and indirectly influences the concentration of guest species (F^- and TPA^+), which could control the process of nucleation and crystal growth and further influences the structure and morphology of zeolite.[50] Fyfe reported the synthesis of MFI zeolite with a morphology of inter-grown obloids under NH_4F and minimal water content gels.[51] In this study, when increasing the H_2O/SiO_2 ratio to 20, the sample presents dispersed plate shape (Figure S1) with larger size (3.8 × 1.8 × 0.35 μm) and lower aspect ratio (AR = 8.0), and some amorphous materials appear leading to low relatively crystallinity (78%). This suggests that high H_2O/SiO_2 ratio gives reduction of F^- and TPA^+ concentration, leads to the increase of its crystal size with length. Optimizing the synthesis composition, a suitable water content combing concentration of F^-/TPA^+ pairs can modify the dissolution and migration of silicon and aluminum species, thus affecting the morphology of the synthesized sample.

With the same synthesis recipe as sample B, crystal growth curves at 373 K and 453 K were compared in Figure 2. When crystallization occurred at 373 K and constant pressure, nucleation induction period was long and crystal growth started after 36 h, the zeolite crystals with high aspect ratio were obtained after 72 h. However, the crystallization rate largely increased while crystallization time decreased at 453 K, and the high crystalline product was obtained after 12 h. An increase in crystallization temperature leads to larger zeolite crystals.[52] As seen in SEM image (Figure S2), the irregular and dispersed crystals still remain lamellar morphology with the larger size of 2.4 × 1.0 × 0.2 μm, showing that the crystal growth increased along the crystal faces corresponding to a*b*c axes. For the resulting material, its crystal size is strongly related to the number and distribution of crystal nucleus in the synthesis gels. When the rapid crystallite growth overuse of precursor species at the high temperature (453 K), the number of nucleation is relatively reduced, leading to the relatively larger crystals. And the number of metastable phase increases at 453 K, thus

obtained crystals become irregular morphology. In contrast, more nuclei evolve at 373 K in the long induction period, and then the crystallite growth starts by employing these viable nuclei to gradually form high crystalline zeolite. So the formation of zeolite with ultimate crystal morphology is mainly governed by the reaction composition and conditions of synthesized system, including the concentration of fluoride ions, water content, crystal temperature and time. Herein, by using solid silica as Si source with relatively dense system, the synthesized process under 373 K crystallization temperature has significant potential for industrial application.

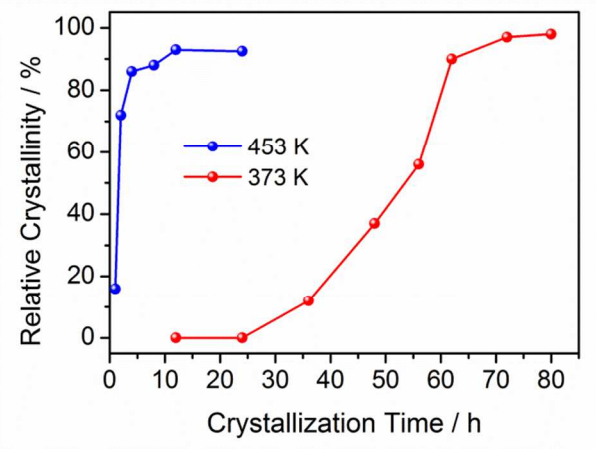

Figure 2. Crystal growth curves of sample B synthesized at different temperatures

3.2 Physicochemical properties of hierarchical ZSM-5 zeolite

To further understand the textural properties of fluoride-prepared ZSM-5 zeolites, the well-crystallized sample B (denoted as M-ZSM-5) and conventional ZSM-5 zeolite (in alkali medium, C-ZSM-5) were comparatively characterized (XRD, Figure S3). The C-ZSM-5 presents cubic shape with size of about 1 μm (SEM, Figure S4).

Figure 3(a) shows TEM image of M-ZSM-5 with hexagonal lamellar morphology. The circular streaking in the SAED pattern (inset of Figure 3(a)) presents that the projection view down the thinner dimension of M-ZSM-5 crystal corresponds to the [010] direction. This gives confirmation that the *b*-axis (the straight channels) is the shortest dimension of the crystal. Furthermore, as seen clearly in Figure 3(b), some randomly distribution mesopores can be observed in the M-ZSM-5 zeolite and the pore diameters are in the range of 10-40 nm.

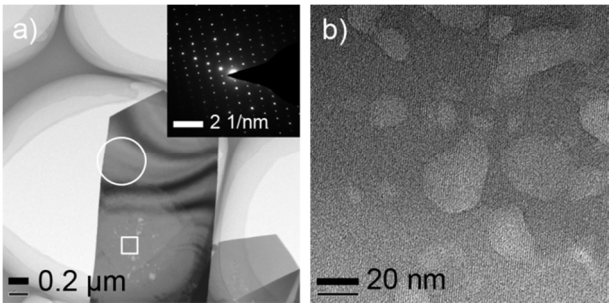

Figure 3. TEM images of M-ZSM-5 sample.

The N_2 adsorption/desorption isotherms and the corresponding pore size distribution of M-ZSM-5 and C-ZSM-5 are shown in Figure 4. Each of the curves has a steep increase at extremely low relative pressure, indicating the nitrogen adsorbed in the uniform micropores. Obviously, the conventional ZSM-5 has a characteristic of traditional microporous materials without mesopore. The isotherm of M-ZSM-5 synthesized by the F-assisted route, significantly different from that of C-ZSM-5, presents a representative modified type IV isotherm, containing an obvious hysteresis loop corresponding to capillary condensation at P/P_0=0.45-0.99, which suggests the irregular mesoporosity arising from the voids between particles.[53] More interestingly, M-ZSM-5 presents a specific hysteresis loop in the range of P/P_0=0.10-0.30, which is usually considered as a fluid-to-crystalline phase transition of adsorbed phase in the micropores.[54, 55] This phase transition phenomenon becomes more pronounced for the high silica MFI zeolite (eg. Silicate-1).[56] For the similar SiO_2/Al_2O_3 of M-ZSM-5 and C-ZSM-5, M-ZSM-5 crystals with lamella-like morphology may be favourable for the phase transition, which is identical with Xiao's report.[31] The pore size distribution curve of M-ZSM-5 indicates that the material has bi-modal porosity including MFI micropore and mesopores within the range of 10-40 nm (inset Figure 4), which is well in agreement with the HRTEM image.

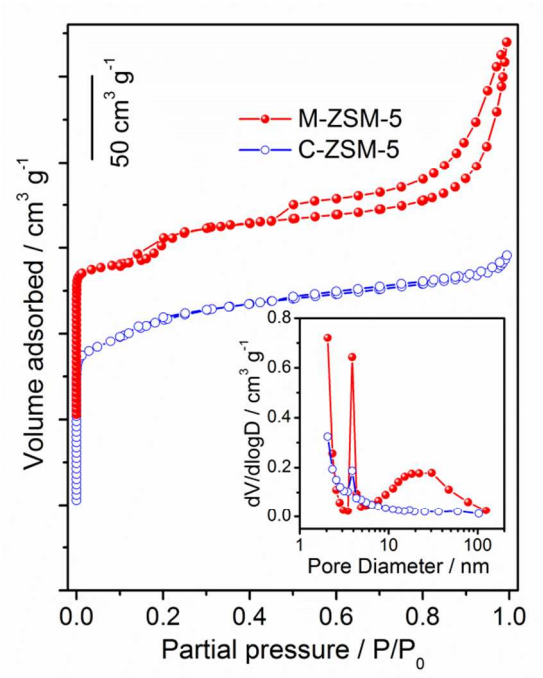

Figure 4. N_2 adsorption/desorption isotherms and BJH pore size distributions of M-ZSM-5 and C-ZSM-5.

The textural properties of the two synthesized ZSM-5 samples are compared in Table 2. The BET surface areas of M-ZSM-5 and C-ZSM-5 are very close, 358 m^2 g^{-1} and 362 m^2 g^{-1}, respectively. But the external surface of M-ZSM-5 is higher (105 m^2 g^{-1}) than that of C-ZSM-5 (87 m^2 g^{-1}), with an increase of 21%. Especially, the total pore and mesopore volume for M-ZSM-5 are 0.33 cm^3 g^{-1} and 0.20 cm^3 g^{-1}, higher than those of C-ZSM-5 (0.22 cm^3 g^{-1} and 0.08 cm^3 g^{-1}). Combining with the N_2 adsorption/desorption isotherms, the larger external surface area and increased pore volume affirmatively result from the creation of mesopores/or voids.

Table 2. Textural properties of M-ZSM-5 and C-ZSM-5

Sample	SiO_2 /Al_2O_3 [a]	S_{BET} [b] [m^2 g^{-1}]	S_{ext} [c] [m^2 g^{-1}]	V_{total} [d] [cm^3 g^{-1}]	V_{meso} [cm^3 g^{-1}]
M-ZSM-5	256	358	105	0.33	0.20
C-ZSM-5	232	362	87	0.22	0.08

[a] SiO_2 /Al_2O_3 molar ratio of the synthesized hierarchical and conventional ZSM-5 zeolite determined by XRF. [b] S_{BET} (BET surface area) obtained from the adsorption isotherm. [c] S_{ext} (external surface areas) calculated using t-plot method. [d] V_{total} (total pore volumes) obtained at P/P_0=0.99.

The NH_3-TPD profiles of M-ZSM-5 and C-ZSM-5 are shown in Figure 5. Two NH_3 desorption peaks could be observed in the temperature regions 440-470 K and 620-660 K, which were attributed to weak and strong acid sites, respectively. As seen, the total area for M-ZSM-5 is considerably close to that for the corresponding catalyst C-ZSM-5, which demonstrates that there is similar density of the acid sites on the two samples. Obviously, there is a significantly difference between the distribution of weak and strong acid sites, that M-ZSM-5 has more weak acid and less strong acid than the C-ZSM-5.

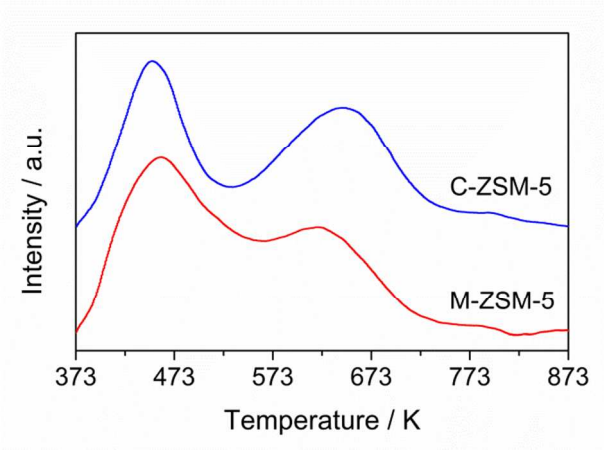

Figure 5. NH_3-TPD profiles of M-ZSM-5 and C-ZSM-5

3.3 Formation mechanism of hierarchical ZSM-5 zeolites

^{19}F MAS-NMR spectrum has been established for understanding of the incorporation of fluorine species into framework during the synthesis. For M-ZSM-5 sample, the spectrum in Figure 6 displays two significant signals at -64 and -140 ppm, along with some weaker peaks at -79, -105 and -129 ppm, etc. The peak at -64 ppm is assigned to fluoride ion in a [$4^1$$5^2$$6^2$] cage due to the fluoride presented as a counterion of TPA^+ and located in framework interstices, and the signal at -140 ppm can be tentatively attributed to AlF_6^{3-} species which presents inside or outside the crystal.[57, 58] While the weak peak at -79 ppm may be associated with defects in the structure, the signal about -129 ppm is presumably assigned to silicofluoro complexes SiF_6^{2-} species, and the broader and weaker signal at -105 ppm could be interpreted as being used to the presence of non-specifically adsorbed F^- (O-H ⋯ F).[58, 59] The result demonstrates that fluoride species in the synthesis system not only perform as charge balance with template agent to contribute to the stabilization of the structure, but ensure the formation of T-F (T: Si, Al) species to encourage the crystallization.

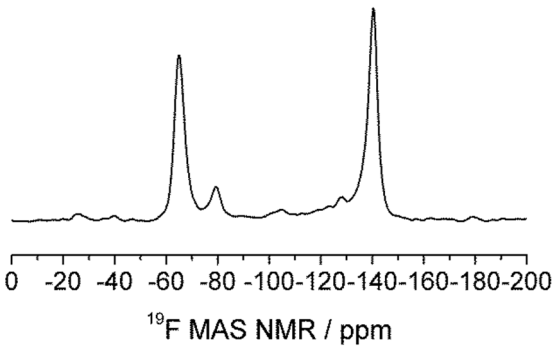

Figure 6. ^{19}F MAS NMR spectrum of the hierarchical ZSM-5 sample synthesized in F^- medium.

Compared to TEOS as silica source in diluted mixture gel system,[34, 41] herein, the use of solid silica source, relatively dense gel and neutral fluoride medium could make the crystallization of M-ZSM-5 quite distinguishable. As above discussion, silica/aluminum species are related to F^- concentration and water content in the synthesis gel, which could modify the structure-directing ability of the F^-/TPA^+ template and control the rate of nucleation and crystallization, thus give a crucial influence on morphology of MFI crystals.

SEM images in Figure 7 primarily describe the formation process of M-ZSM-5 during different period of crystallization at 373 K. In the initial stage of crystallization (12 h), large particles are obtained from the mixture gels (Figure 7(a)) and no obvious crystalline phase is observed at XRD patterns (Figure S5). According to its crystallization curve, it is suggested that silica sparingly dissolves and some solid maintains in the induction stage. After 36 h, a large number of small particles or platelets are observed (Figure 7(b)), showing weak XRD diffraction peaks at 2θ = 7-9° and 22.5-25°, which suggests that more solid silica dissolve and start to form the elementary units of ZSM-5. As time prolonged to 56 h, some thinner plates around 1 μm size with the relative crystallinity of ~54% are clearly observed in Figure 7(c), indicating the formation of ZSM-5 crystals. The amorphous silica/ alumina species are completely disappeared and highly crystalline ZSM-5 zeolite with lamellar morphology (Figure 7(d)) is fully accomplished after 72 h. This growth process is consistent with the crystallization curves in Figure 2 and the N_2 analysis isotherms over the resulting materials in Figure S6. At the crystallization time of 12 h and 36 h, the material presents a hysteresis loop from N_2 analysis at P/P_0 above 0.8 featuring large mesopores/macropores structure mainly arising from the raw materials. With crystallization time increasing to 56 h, a hysteresis loop occurs at about 0.45 relative pressure which is associated with the presence of mesopores. Finally, two hysteresis loops at P/P_0=0.1-0.25 and 0.45-0.99 were found which are closely related to obtained hierarchical M-ZSM-5 zeolite.

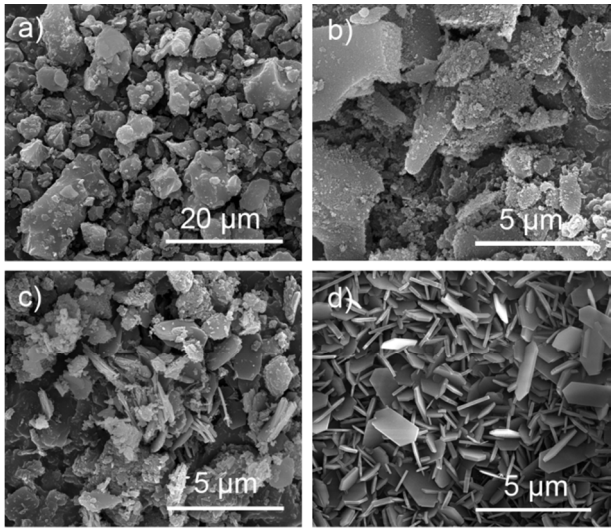

Figure 7. SEM images of M-ZSM-5 during the crystallization stage: a) 12 h; b) 36 h; c) 56 h; d) 72 h.

The primary synthesis mechanism of ZSM-5 is described in the Scheme 1. At the beginning, the solid silica materials partially solubilize under near-neutral pH value and low crystallization temperature, simultaneously, fluoride and template TPA^+ spontaneously disperse into the solid silica support due to the increase of entropy.[60, 61] On the one hand, fluorine acts as the template with the ions-pair form (F^--TPA^+) inside the [$4^1$$5^2$$6^2$] cage in MFI channels and creates a covalent bond with Si to form an energetically stable $[SiO_{4/2}F]^-$ unit by the high electronegativity,[62] improving the dissolution of silica species and the formation of T-O-T (T: Si or Al) bonds.[63] On the other hand, the neighboring silicon and aluminum raw materials around fluoride ions gradually form Si-F and Al-F complex, and thus these complex species self-organize to form a local reservoirs of nucleus.[34] With the dissolution of the solid silica sources and the formation of large number of nuclei, these aluminosilicate species are locally rearranged to form MFI nanocrystals. Due to the electronic interaction among fluoride ions, TPA^+ and Si species (which significantly influences on the morphology), zeolite crystals grow along defined spatial direction.[64] Numerous nanocrystals are condensed and finally constantly consume neighbor solid silica/aluminum species to form lamellar MFI crystals with preferential *b*-orientation. Under the dense system with low water content, the silicon and aluminum species is difficult to migrate in the synthesis gels. The assembly of aluminosilicate species around TPA^+ is non-uniform, resulting in the presence of some mesopores in the surface or interior of MFI crystals. In addition, large amount of AlF_6^{3-} and SiF_6^{2-} species are present inside or outside the synthesized crystals and almost completely removed by calcined (XPS spectra in Figure S7). Therefore, it is speculate that the mesoporous structure of M-ZSM-5 might be created from the platelets dislocation during crystallization process and partly from the post-treatment during the removal of Si-F and Al-F complex by calcination or ion-exchange.

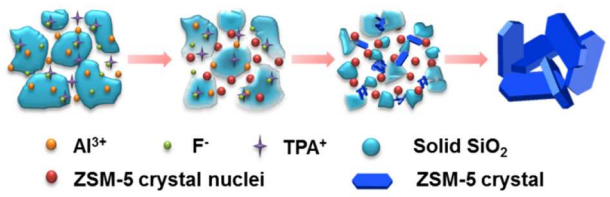

Scheme 1. The proposed approach for the formation of ZSM-5 zeolite under F medium.

3.4 Catalytic performance of hierarchical ZSM-5 zeolites

The hierarchical ZSM-5 (M-ZSM-5) and the conventional ZSM-5 (C-ZSM-5) are comparatively evaluated for MTP reaction. The catalytic activity of M-ZSM-5 and C-ZSM-5 as a function of time displays in Figure 8. At the beginning reaction, methanol conversion over both samples is approximately 100%, but the reactive stability over M-ZSM-5 presents more prominent. When the catalyst deactivation is set as methanol conversion from 100% falling to around 90%, the catalytic lifetime of M-ZSM-5 (224 h) is nearly twice as longer as that of C-ZSM-5 (98 h).

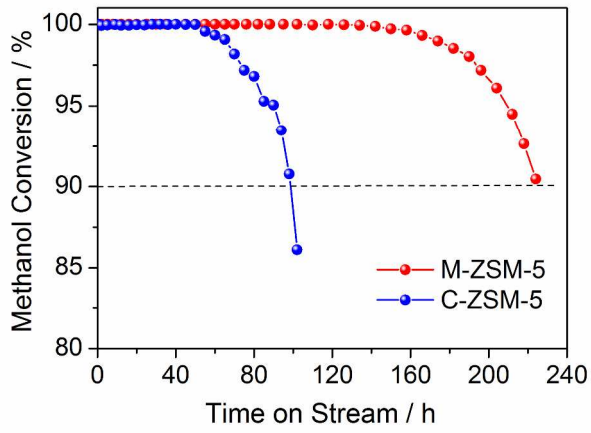

Figure 8. Methanol conversion with time on stream over M-ZSM-5 and C-ZSM-5 catalysts. *Reaction condition: T* = 743 K, *P* = 0.1 MPa, $n(CH_3OH) : n(H_2O)$ = 1:1, *WHSV* = 3.0 h^{-1}.

Figure 9 exhibits the product distribution over sample M-ZSM-5 and C-ZSM-5 as function of TOS. At the initial stage (TOS=0.5), the propylene and butylene selectivity are amount to 42.7% and 28.8% for M-ZSM-5, remarkably higher than those of C-ZSM-5 (33.3% and 21.2%), but the selectivity to ethylene is lower. After about 20 h TOS, the reaction reached the steady state with the stable products selectivity over the two ZSM-5 catalysts. Both samples exhibit regular catalytic behaviour with TOS for the target products, involving the steady formation of propylene, a gradual decrease of ethylene and butylene and a gradual increase of C_{5+} compounds. Obviously, M-ZSM-5 maintains stable performance for a longer period of more than 200 h, and the steady stage for C-ZSM-5 is only 80 h. The average value of product selectivity at steady stage is shown in Figure S8. Compared to C-ZSM-5, M-ZSM-5 zeolite shows higher selectivity towards propylene (45.1% *vs.* 38.1%) and butylene (27.2% *vs.* 21.3%), lower selectivity towards ethylene (6.5% *vs.* 9.2%), leading to higher propylene/ethylene ratio (P/E) (6.91 *vs.* 4.15). And the total light olefins ($C_2^=$-$C_4^=$) over M-ZSM-5 is nearly to 80%, which is greatly higher than that of C-ZSM-5. Furthermore, M-ZSM-5 allows lower C_1-C_4 alkanes and C_{5+} hydrocarbons. With prolonged reaction time, the catalysts deactivated and the methanol conversion drops rapidly. Close to the deactivation stage, the propylene selectivity decreased slowly and the C_{5+} increased greatly. It is accepted that the deactivation of catalyst in MTP process generally arises from coke deposition.[65] As shown in Figure S9, M-ZSM-5 contains 8.48 wt.% coke deposit after 224 h on stream, while for C-ZSM-5 the coke deposit is 11.34 wt.% after 98 h. Owing to low coke deposition, M-ZSM-5 presents longer catalytic lifetime than C-ZSM-5.

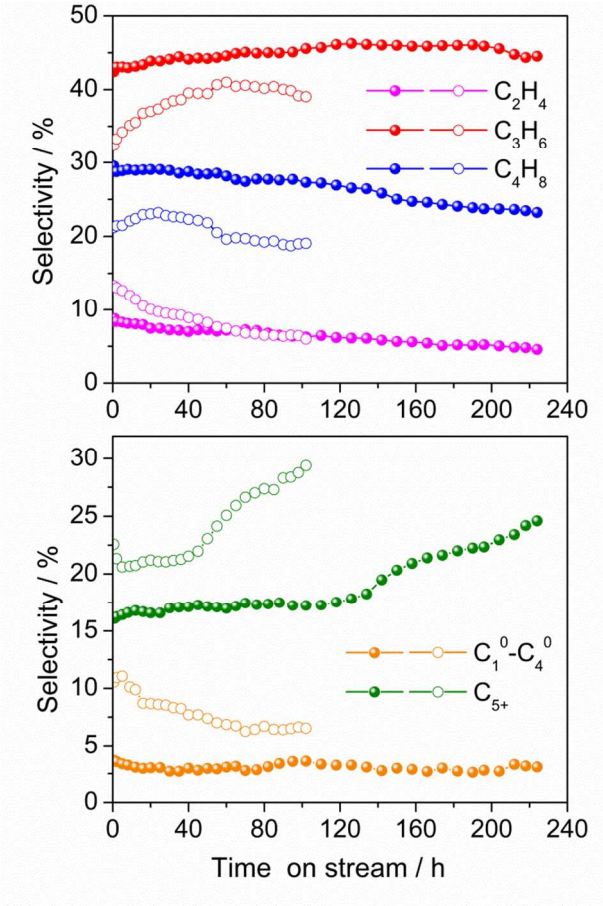

Figure 9. Product selectivity of M-ZSM-5 (filled symbols) and C-ZSM-5 (open symbols) for MTP reaction as time on stream. *Reaction condition: T* = 743 K, *P* = 0.1 MPa, $n(CH_3OH) : n(H_2O)$ = 1:1, *WHSV* = 3.0 h^{-1}.

According to the "dual-cycle" MTO/P reaction mechanism, the formation of propylene and butylene is govern by alkenes methylation/cracking pathway whereas ethylene is mainly formed through aromatics/ethylene cycle, and the aromatics/ethylene cycle cannot run without the C_{3+} alkenes cycle.[12] For the solid-acid catalytic reaction, the acidic property

over ZSM-5 zeolite affects the activity and selectivity during MTP process. It is accepted that the strong acidity is regarded as the main active sites for the conversion of methanol, but they also can accelerate the formation of coke species through secondary reactions.[66] The weak acidity promotes methylation and alkylation reactions, which is favourable for the formation of alkene-intermediate.[67, 68] Moreover, the weak acidity can restrain hydrogen-transfer reactions to produce saturated hydrocarbons and aromatics, which are the precursors for coke formation.[69] Therefore, the appropriate weak acid density is benefit to facilitate the formation of olefins and reduce the further reactions for hindering coke deposition.[70] As a result, M-ZSM-5 obtained form fluoride system holding less strong and more weak acidity has good activity for the C_{3+} alkenes cycle in MTP reaction, thus leading to higher propylene selectivity. And also, the lifetime of M-ZSM-5 is remarkably enhanced due to less coke deposition.

Besides the proper catalytic acidity, the high propylene selectivity and long catalytic lifetime strongly depend on the enhanced diffusivity in the zeolite.[14] The hierarchical M-ZSM-5 zeolite can facilitate the removal of light olefins (in particular propylene and butylene) from the channels. With the improvement of diffusivity, the residence time of the primary olefin products is reduced and secondary reactions (alkylation, cracking, hydrogen transfer and cyclization) are restrained, which are benefit to suppress the aromatic/ethylene cycle and reduce the formation of coke species. Combing the thinner thickness (~100 nm) along *b* axis and introduced mesopores in M-ZSM-5, which shorten the diffusion path length and increase opening mouths, high propylene and butylene selectivity and long catalytic life time are observed in MTP reaction. And also, secondary reactions for coke deposition would be suppressed on M-ZSM-5, leading to low selectivities of C_1^0-C_4^0 and C_{5+} hydrocarbons.

4. Conclusions

In summary, the hierarchical ZSM-5 zeolite (M-ZSM-5) with thinner *b*-oriented morphology has been obtained in fluoride medium by using solid silica with dense gels at 373 K. Influencing parameters, such as fluoride concentration, water content, crystallization temperature and time, are critical factors for the control of crystallographic morphology and size. The obtained material with thickness of 100 nm possesses abundant mesopores, resulting in higher external surface and extremely larger volume. Moreover, the synthesis mechanism of M-ZSM-5 is discussed. Fluoride ions with strong electronegativity promote the dissolution of solid silica and act as the structure directing agent in the form of ions-pair (F^--TPA^+), leading to the formation of ZSM-5 nuclei /microcrystals. These microcrystals gradually generate the platelets and fabricate the hierarchical ZSM-5 zeolite with thinner *b*-axis oriented dimension.

Compared to C-ZSM-5 sample, M-ZSM-5 zeolite performs longer catalytic lifetime in MTP reaction. The initial propylene and butylene selectivity over M-ZSM-5 zeolite increase by 9.4 % and 7.6 %, respectively. And the selectivity of propylene and butylene are more than 45% and 27%, the total olefins (ethylene, propylene and butylene) selectivity is nearly 80% at the steady stage. The excellent performance should be contributed to its optimal acidity and the superior diffusivity for the specific structure with thinner *b*-axis path and intracrystal secondary mesopores.

Acknowledgements

The authors acknowledge the State Key Development Program for Basic Research of China (2012CB215002) and the National Natural Science Foundation of China (21176255, 21276278) for the financial support of this work.

Notes and references

[a]State Key Laboratory of Heavy Oil Processing, The Key Laboratory of Catalysis of CNPC, China University of Petroleum-Beijing, Beijing, China. E-mail: gongyj@cup.edu.cn; Fax: +86 10 8973 4979; Tel: +86 10 8973 3066

[b]State Key Laboratory of Magnetic Resonance and Atomic and Molecular Physics, Wuhan Center for Magnetic Resonance, Wuhan Institute of Physics and Mathematics, Chinese Academy of Sciences, Wuhan, China

†Electronic Supplementary Information (ESI) available: SEM images of ZSM-5 synthesized with different factors; XRD patterns of ZSM-5 zeolite synthesized in F^- and OH^- medium; XRD patterns and N_2 adsorption/desorption isotherms of M-ZSM-5 obtained at different crystallization times; product selectivity for MTP reaction and thermogravimatric curves of the deactivated zeolites are provided in the Figure S1-S9. See DOI: 10.1039/b000000x/

1 C. D. Chang, *Catal. Rev.*, 1983, **25**, 1-118.
2 F. J. Keil, *Micropor. Mesopor. Mater.,* 1999, **29**, 49-66.
3 U. Olsbye, S. Svelle, M. Bjørgen, P. Beato, T. V. W. Janssens, F. Joensen, S. Bordiga and K. P. Lillerud, *Angew. Chem. Int. Ed.*, 2012, **51**, 5810-5831.
4 C. D. Chang, C. T. W. Chu and R. F. Socha, *J. Catal.*, 1984, **86**, 289-296.
5 M. Stöcker, *Micropor. Mesopor. Mater.,* 1999, **29**, 3-48.
6 J. F. Haw, W. Song, D. M. Marcus and J. B. Nicholas, *Acc. Chem. Res.*, 2003, **36**, 317-326.
7 C. Wang , Y. Chu , A. Zheng, J. Xu, Q. Wang, P. Gao, G. Qi, Y. Gong and F. Deng, *Chem.–Eur. J.*, 2014, **20**, 12432-12443.
8 S. Müller, Y. Liu, M. Vishnuvarthan, X. Sun, A. C. van Veen, G. L. Haller, M. Sanchez-Sanchez and J. A. Lercher, *J. Catal.*, 2015, **325**, 48-59.
9 R. Khare, D. Millar and A. Bhan, *J. Catal.*, 2015, **321**, 23-31.
10 Q. Wang, S. Xu, J. Chen, Y. Wei, J. Li, D. Fan, Z. Yu, Y. Qi, Y. He, S. Xu, C. Yuan, Y. Zhou, J. Wang, M. Zhang, B. Su and Z. Liu, *RSC Adv.*, 2014, **4**, 21479-21491.
11 Q. Zhang, S. Hu, L. Zhang, Z. Wu, Y. Gong and T. Dou, *Green Chem.*, 2014, **16**, 77-81.
12 S. Svelle, F. Joensen, J. Nerlov, U. Olsbye, K.-P. Lillerud, S. Kolboe and M. Bjørgen, *J. Am. Chem. Soc.*, 2006, **128**, 14770-14771.

13 M. Bjørgen, S. Svelle, F. Joensen, J. Nerlov, S. Kolboe, F. Bonino, L. Palumbo, S. Bordiga and U. Olsbye, *J. Catal.*, 2007, **249**, 195-207.
14 C. Mei, P. Wen, Z. Liu, H. Liu, Y. Wang, W. Yang, Z. Xie, W. Hua and Z. Gao, *J. Catal.*, 2008, **258**, 243-249.
15 J. Kim, M. Choi and R. Ryoo, *J. Catal.*, 2010, **269**, 219-228.
16 A. Corma, *Chem. Rev.*, 1997, **97**, 2373-2420.
17 L. H. Chen, X. Y. Li, J. C. Rooke, Y. H. Zhang, X. Y. Yang, Y. Tang, F. S. Xiao and B. L. Su, *J. Mater. Chem.*, 2012, **22**, 17381.
18 D. H. Olson, G. T. Kokotailo, S. L. Lawton and W. M. Meier, *J. Phys. Chem.*, 1981, **85**, 2238-2243.
19 J. Caro, M. Noack, J. Richter Mendau, F. Marlow, D. Petersohn, M. Griepentrog and J. Kornatowski, *J. Phys. Chem.*, 1993, **97**, 13685-13690.
20 G. Muller, T. Narbeshuber, G. Mirth and J. A. Lercher, *J. Phys. Chem.*, 1994, **98**, 7436-7439.
21 L. Gueudré, T. Binder, C. Chmelik, F. Hibbe, D. M. Ruthven and J. Kärger, *Materials*, 2012, **5**, 721-740.
22 M. Choi, K. Na, J. Kim, Y. Sakamoto, O. Terasaki and R. Ryoo, *Nat. Mater.*, 2009, **461**, 246-249.
23 K. Na, M. Choi, W. Park, Y. Sakamoto, O. Terasaki and R. Ryoo, *J. Am. Chem. Soc*., 2010, **132**, 4169-4177.
24 S. Hu, J. Shan, Q. Zhang, Y. Wang, Y. Liu, Y. Gong, Z. Wu and T. Dou, *Appl. Catal. A-Gen.*, 2012, **445-446**, 215-220.
25 M. Tsapatsis, *AIChE J.*, 2014, **60**, 2374-2381.
26 R. Mostowicz and J. M. Berak, in *Stud. Surf. Sci. Catal.*, Elsevier, 1985, **24**, 65-72.
27 L. F. Petrik, C. T. O'Connor and S. Schwarz, in *Stud. Surf. Sci. Catal.*, Elsevier, 1995, **94**, 517-524.
28 G. Bonilla, I. Díaz, M. Tsapatsis, H. K. Jeong, Y. Lee and D. G. Vlachos, *Chem. Mater.*, 2004, **16**, 5697-5705.
29 X. Chen, W. Yan, X. Cao, J. Yu and R. Xu, *Micropor. Mesopor. Mater.,* 2009, **119**, 217-222.
30 Z. C. Shan, H. Wang, X. J. Meng, S. Y. Liu, L. A. Wang, C. Y. Wang, F. Li, J. P. Lewis and F. S. Xiao, *Chem. Commun.,* 2011, **47**, 1048-1050.
31 Y. Liu, X. Zhou, X. Pang, Y. Jin, X. Meng, X. Zheng, X. Gao and F. S. Xiao, *ChemCatChem*, 2013, **5**, 1517-1523.
32 P. Caullet, J. L. Paillaud, A. Simon-Masseron, M. Soulard and J. Patarin, *C. R. Chim.*, 2005, **8**, 245-266.
33 C. A. Fyfe, D. H. Brouwer, A. R. Lewis, L. A. Villaescusa and R. E. Morris, *J. Am. Chem. Soc.*, 2002, **124**, 7770-7778.
34 J. Arichi and B. Louis, *Cryst. Growth. Des.*, 2008, **8**, 3999-4005.
35 B. Louis and L. K. Minsker, *Micropor. Mesopor. Mater.,* 2004, **74**, 171-178.
36 H. Yu, X. Wang and Y. Long, *Micropor. Mesopor. Mater.,* 2006, **95**, 234-240.
37 M. E. Dose, K. Zhang, J. A. Thompson, J. Leisen, R. R. Chance, W. J. Koros, B. A. McCool and R. P. Lively, *Chem. Mater.*, 2014, **26**, 4368-4376.
38 X. Q. Yao, X. Y. Xu, Z. Lu, K. Jiao, J. Q. Song, Z. F. Li, Q. Wang, L. J. Yan and M. Y. He, *Acta Phys-Chim Sin.*, 2013, **29**, 1809-1813.
39 S. Ivanova, C. Lebrun, E. Vanhaecke, C. Pham-Huu and B. Louis, *J. Catal.*, 2009, **265**, 1-7.
40 F. L. Bleken, S. Chavan, U. Olsbye, M. Boltz, F. Ocampo and B. Louis, *Appl. Catal. A-Gen.*, 2012, **447-448**, 178-185.
41 Z. Qin, L. Lakiss, L. Tosheva, J.-P. Gilson, A. Vicente, C. Fernandez and V. Valtchev, *Adv. Funct. Mater.*, 2014, **24**, 257-264.
42 H. Lechert, *Micropor. Mesopor. Mater.,* 1998, **22**, 519-523.
43 J. L. Guth, H. Kessler, J. M. Higel, J. M. Lamblin, J. Patarin, A. Seive, J. M. Chezeau and R. Wey, in *Zeolite Synthesis*, American Chemical Society, 1989, **398**, 176-195.
44 L. Wang, Y. Shao, J. Zhang and M. Anpo, *Micropor. Mesopor. Mater.,* 2007, **100**, 241-249.
45 J. D. H. Donnay and D. Harker, *Am. Mineral*, 1937, **22**, 446-467.
46 P. Hartman and W. Perdok, *Acta Crystallogr*, 1955, **8**, 49-52.
47 J. H. Koegler, H. van Bekkum and J. C. Jansen, *Zeolites*, 1997, **19**, 262-269.
48 D. G. Hay, H. Jaeger and K. G. Wilshier, *Zeolites*, 1990, **10**, 571-576.
49 T. Ban, H. Mitaku, C. Suzuki, J. Matsuba, Y. Ohya and Y. Takahashi, *J Cryst Growth*, 2005, **274**, 594-602.
50 M. A. Camblor, L. A. Villaescusa and M. J. Díaz-Cabañas, *Top. Catal.*, 1999, **9**, 59-76.
51 C. A. Fyfe, R. J. Darton, H. Mowatt and Z. S. Lin, *Micropor. Mesopor. Mater.,* 2011, **144**, 57-66.
52 C. S. Cundy, B. M. Lowe and D. M. Sinclair, *Faraday Discuss.*, 1993, **95**, 235-252.
53 N. Alam and R. Mokaya, *Micropor. Mesopor. Mater.,* 2011, **143**, 104-114.
54 P. L. Llewellyn, J. P. Coulomb, Y. Grillet, J. Patarin, G. Andre and J. Rouquerol, *Langmuir*, 1993, **9**, 1852-1856.
55 G. Kyriakou and C. R. Theocharis, in *Stud. Surf. Sci. Catal.*, Elsevier, 2002, **144**, 709-716.
56 U. Müller and K. K. Unger, in *Stud. Surf. Sci. Catal.*, Elsevier, 1988, **39**, 101-108.
57 L. Delmotte, M. Soulard, F. Guth, A. Seive, A. Lopez and J. L. Guth, *Zeolites*, 1990, **10**, 778-783.
58 J. L. Guth, L. Delmonte, M. Soulard, B. Brunard, J. F. Joly and D. Espinat, *Zeolites*, 1992, **12**, 929-935.
59 J. I. Corredor, A. Cota, E. Pavon and M. D. Alba, *Am. Mineral.*, 2013, **98**, 1000-1007.
60 F. S. Xiao, S. Zheng, J. Sun, R. Yu, S. Qiu and R. Xu, *J. Catal.*, 1998, **176**, 474-487.
61 L. Ren, Q. Wu, C. Yang, L. Zhu, C. Li, P. Zhang, H. Zhang, X. Meng and F. S. Xiao, *J. Am. Chem. Soc.*, 2012, **134**, 15173-15176.
62 C. A. Fyfe, D. H. Brouwer, A. R. Lewis and J.-M. Chézeau, *J. Am. Chem. Soc.*, 2001, **123**, 6882-6891.
63 B. Louis, G. Laugel, P. Pale and M. M. Pereira, *ChemCatChem*, 2011, **3**, 1263-1272.
64 K. B. Yoon, *Acc. Chem. Res.*, 2007, **40**, 29-40.
65 F. Schmidt, C. Hoffmann, F. Giordanino, S. Bordiga, P. Simon, W. Carrillo-Cabrera and S. Kaskel, *J. Catal.*, 2013, **307**, 238-245.
66 F. Yaripour, Z. Shariatinia, S. Sahebdelfar and A. Irandoukht, *Micropor. Mesopor. Mater.,* 2015, **203**, 41-53.
67 Y. Yang, C. Sun, J. Du, Y. Yue, W. Hua, C. Zhang, W. Shen and H. Xu, *Catal. Commun*, 2012, **24**, 44-47.
68 M. Westgård Erichsen, S. Svelle and U. Olsbye, *Catal. Today*, 2013, **215**, 216-223.
69 Q. Zhu, J. N. Kondo, T. Setoyama, M. Yamaguchi, K. Domen and T. Tatsumi, *Chem. Commum.*, 2008, **41**, 5164-5166.
70 S. Zhang, Y. Gong, L. Zhang, Y. Liu, T. Dou, J. Xu and F. Deng, *Fuel Process. Technol.*, 2015, **129**, 130-138.

Graphical Abstract

F-assisted Synthesis of Hierarchical ZSM-5 Zeolite for Methanol to Propylene Reaction: *b*-Oriented Thinner Dimensional Morphology

Lanlan Zhang,[a] Yu Song,[a] Guodong Li,[a] Qing Zhang,[a] Shaolong Zhang,[a] Jun Xu,[b] Feng Deng,[b] and Yanjun Gong*[a]

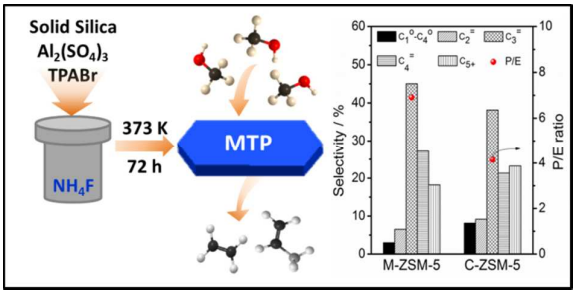

Hierarchical ZSM-5 zeolite with thinner dimension morphology has been synthesized in fluoride medium, which presents superior performance in MTP reaction.